IAC-25.A6.4.10

End-of-Life disposal design for Near-Rectilinear Halo Orbits

Mathilda Bolis [a,*], Elisa Maria Alessi[b], Camilla Colombo [a]

[a] *Department of Aerospace Science and Technology, Politecnico di Milano, Via La Masa 34, 20156, Milan, Italy. mathilda.bolis@polimi.it, camilla.colombo@polimi.it*
[b] *Istituto di Matematica Applicata e Tecnologie Informatiche "Enrico Magenes", Consiglio Nazionale delle Ricerche, Via Alfonso Corti 12, Milano, 20133, Italy em.alessi@mi.imati.cnr.it*
[*]Corresponding author: mathilda.bolis@polimi.it

Abstract

In recent years, there has been a clear increase in space traffic in the cislunarregion, which is expected to become even more pronounced in the future. Given the space debris problem we are facing in near-Earth space and the importance of the cislunarregion, the current plans aim to avoid the same issue from occurring between the Earth and the Moon. To this end, one of the best mitigation strategies to implement is careful planning of End-of-Life (EoL) disposal solutions.

To do so would require providing accurate, low-cost disposal options in an efficient and customised manner. Current research on EoL disposal in cislunarspace focuses mainly on studying the problem with a probabilistic approach, for example, to estimate the effect of uncertainties on the system. We propose instead to address the problem of disposal design for cislunarspace by leveraging the system dynamics to minimise the ΔV cost.

This work aims to design and compare disposal strategies for Near-Rectilinear Halo Orbits (NRHOs) in Earth-Moon (EM) L_1 and L_2. These orbits were chosen for the analysis as they are of particular interest for many future missions, such as, for example, the lunarGateway. Of the four disposal strategies usually considered when planning the EoL phase of a mission in cislunarspace, two were selected as the most suitable for these orbits: disposal with insertion on a heliocentric no-return orbit and lunar impact. The former was chosen as it is low-cost and reliable, if supported by long-term simulations. In this case, the disposal trajectory is designed using an energetic approach, which involves a two-impulse manoeuvre: the first in the direction of the unstable manifold and the second to close the Zero Velocity Curves (ZVCs) of the Sun-Earth (SE) system. The latter of the two strategies is chosen due to the natural proximity of NRHOs to the lunar surface. The EoL phase is defined by looking for solutions where the CR3BP dynamics can be exploited to find passive solutions. The disposal trajectory is then optimised to minimise the disposal cost while ensuring lunar historical sites and protected zones on the Moon's surface are preserved.

By comparing the two strategies, it is defined which is the most convenient to be applied to NRHOs, highlighting which parameters influence the analysis, such as cost, total time needed for the EoL phase and eventual sensitivity to perturbations.

Keywords: cislunarspace, low-cost disposal design, Circular Restricted Three Body Problem, Near-Rectilinear Halo Orbits

Nomenclature

α [°]	Phase defining the geometric relationship between the EM and the SE system
ΔV [m/s]	Characteristic velocity increment
μ [-]	Non-dimensional gravitational constant
$\boldsymbol{r}$ [ndL]	Spacecraft position vector
$\boldsymbol{v}$ [ndL]	Spacecraft velocity vector
U [-]	CR3BP potential-like function
l_{EM} [km]	EM system characteristic length
l_{SE} [km]	SE system characteristic length
r_p [km]	Perilune radius
t [ndT]	Time
ω_{EM} [1/ndT]	Angular velocity of the rotating EM system
ω_{SE} [1/ndT]	Angular velocity of the rotating SE system

Acronym/Abbreviations

BR4BP	Bicircular Restricted Four-Body Problem
COSPAR	Committee on Space Research

CR3BP	Circular Restricted Three Body Problem
EM	Earth-Moon
EoL	End-of-Life
EoM	Equations of Motion
ESA	European Space Agency
JC	Jacobi Constant (JC)
L_1	First collinear Lagrangian point
L_2	Second collinear Lagrangian point
LROC	lunarReconnaissance Orbiter Camera
ME/PA	Mean-Earth/Principal-Axis
NRHO	Near-Rectilinear Halo Orbit
ndL	non-dimensional Length
ndT	non-dimensional Time
PSR	Permanently Shadowed Regions
SE	Sun-Earth
SI	Stability Index
SQP	Sequential Quadratic Programming
ToF	Time of Flight
ZVC	Zero Velocity Curve

1. Introduction

In the coming years, space traffic in the cislunar environment is expected to increase significantly. This region, strongly influenced by the combined gravitational dynamics of the Earth and the Moon, is commonly defined as extending from the high geostationary region up to the Earth–Moon (EM) Lagrangian points, and numerous missions are already planned to operate in this area in the near future. A renewed space era is underway: large-scale programs, such as the lunar Gateway [1], part of NASA's Artemis [2] missions, are being developed in parallel with smaller, less ambitious, yet equally important, missions. The cislunar environment is of unquestionable scientific interest, yet many of its dynamical and environmental characteristics remain not fully understood. What makes operating in this region particularly challenging is not only the greater distance from Earth compared to near-Earth missions, but also the strongly non-linear dynamics governing spacecraft motion under the influence of multiple celestial bodies and effects of non-gravitational perturbations.

In parallel, the international awareness of space as a finite resource is steadily increasing. Just as the Earth's biosphere must be preserved from overexploitation, the same principle applies to near-Earth space. The rapid growth in space missions over the last decade has highlighted how an exponential increase in launches and spacecraft operations inevitably leads to an overuse of this limited resource, gradually threatening the long-term sustainability of space activities. Managing the debris problem is already a significant challenge in near-Earth space, posing great risks to both current and future missions. Since a large number of missions are planned in the next few years, the same concern applies to the cislunar environment, where the issue would be even more complex to manage due to the highly non-linear and chaotic nature of this dynamical region. The most effective way to address the debris issue in cislunarspace is to prevent it from arising in the first place. This can only be achieved through the careful planning of precise and cost-effective mitigation strategies, and, among the possible options, the accurate design of reliable and low-cost disposal trajectories remains the most promising and practical solution.

Four disposal strategies are to be considered when planning the End-of-Life (EoL) phase of a mission orbiting in cislunar space. According to [3], disposal plans for spacecraft operating in lunar orbits shall include one of the following strategies "in order of preference: heliocentric disposal, lunar impact, Earth re-entry, or a lunar graveyard orbit." All disposal strategies should be validated through propagation in an ephemeris-based dynamical model. In cases where a direct impact is not achieved, the spacecraft trajectory must be evaluated for at least 100 years to compute the probability of Earth or Moon re-entry, and associated impact areas, after disposal. Moreover, disposal strategies must not only comply with safety standards to avoid interference with both current and future missions, but also be tailored to the characteristics of the specific operational orbit under consideration.

In this work, Near Rectilinear Halo Orbits (NRHOs) are considered as a reference case for the development of disposal strategies. NRHOs belong to the Halo family and are characterised by a proximity to the Moon as well as a higher degree of linear stability compared to other members of the same family. These two features make NRHOs particularly attractive both for scientific missions dedicated to lunar observation and for crewed missions aiming at lunar exploration. Indeed, a NRHO has been selected as the target orbit for the Lunar Gateway, and the same is foreseen within the Artemis program. Consequently, NRHOs are of high relevance not only from a dynamical perspective but also from an operational mission design standpoint. Among all orbits in cislunar space, they are some of the more interesting to study from a disposal point of view. Given their characteristics, two of the four disposal strategies mentioned above appear especially suitable for NRHOs: heliocentric no-return disposal and controlled lunar impact.

Heliocentric no-return disposal involves designing trajectories that depart from the NRHO, cross the EM L_2 point, and continue towards the Sun–Earth (SE) L_1 or L_2 bottleneck region, ultimately exiting the Zero Velocity Curves (ZVCs) of the SE system. This approach has been extensively studied in relation to periodic orbits in the SE system [4], but its application to the EM case introduces additional challenges [5], particularly due to the coupled influence of the Sun and the Moon. Its main advantage lies in the absence of any collision: no debris or ejecta are generated, and long-term safety is ensured provided that the spacecraft is forced outside the EM

neighbourhood for at least 100 years.
Controlled lunar impact, on the other hand, is an appealing solution for NRHOs due to their inherent proximity to the Moon. Such a strategy would enable fast and low-cost disposal, two highly desirable features, making it a practical choice even when resources to allocate to EoL operations are low. However, this strategy requires careful planning to avoid impact with historical landing sites and other protected lunarregions.
In this paper, these two strategies are compared in terms of operational complexity, end-of-life trajectory design, required ΔV, and disposal time. Furthermore, a set of key parameters expected to strongly influence the outcome of the analysis is identified and would be examined in greater detail in future work.

2. Dynamical model

The Circular Restricted Three-Body Problem (CR3BP) [6] describes the trajectory of a massless object influenced by the gravitational forces of two primary bodies, such as the Earth and the Moon, or the Sun and the Earth, which move in circular orbits around their mutual centre of mass. The vector $\boldsymbol{r} = [r_x, r_y, r_z]$ represents the position, while $\boldsymbol{v} = [v_x, v_y, v_z]$ denotes the velocity, both relative to a rotating coordinate system. In this system, the primaries lie along the x-axis, which has its origin at their centre of mass, with the positive direction pointing toward the smaller primary. The z-axis is orthogonal to the plane of their motion, and the y-axis completes the right-handed coordinate system. The CR3BP is governed by the following Equations of Motion (EoMs):

$$\begin{cases} \dot{r} = v \\ \dot{v} = 2 \begin{bmatrix} v_y \\ -v_x \\ 0 \end{bmatrix} + \nabla_r U \end{cases} \tag{1}$$

where the potential-like function U is defined as:

$$U(\boldsymbol{r}) = \frac{1}{2}(r_x^2 + r_y^2) + \frac{1-\mu}{r_1} + \frac{\mu}{r_2} + \frac{1}{2}\mu(1-\mu) \tag{2}$$

The dimensionless gravitational constant is denoted by μ and in the EM system it has a value of 0.01215, in the SE system of 3.0404×10^{-6}. The variables r_1 and r_2 represent the distances from the third body to the two primary bodies. Here, the larger primary is stationed at $x = -\mu$, and the smaller at $x = 1 - \mu$. Thus, r_1 and r_2 can be expressed as:

$$r_1 = ((r_x + \mu)^2 + r_y^2 + r_z^2)^{1/2} \tag{3}$$

$$r_2 = ((r_x - 1 + \mu)^2 + r_y^2 + r_z^2)^{1/2} \tag{4}$$

All quantities are treated as dimensionless: lengths are scaled relative to the average Earth-Moon or Sun-Earth distance, and time such that the average angular velocity of the rotating frame equals 1. Thus, dimensionless lengths are expressed in units of ndL, standing for non-dimensional length, and dimensionless times are expressed in units of ndT, standing for non-dimensional time. Within the CR3BP, only one integral of motion exists. This integral, termed the Jacobi Constant (JC), is given by:

$$JC(\boldsymbol{r}, \boldsymbol{v}) = 2\bar{U}(\boldsymbol{r}) - ||\boldsymbol{v}||^2 \tag{5}$$

where $\bar{U}(\boldsymbol{r})$ is equal to $U(\boldsymbol{r})$ without the constant term.
According to this definition, if JC increases, the system's energy decreases, and vice versa. In the CR3BP, five equilibrium points, known as the Libration or Lagrange points L_1 to L_5, can be determined, together with periodic solutions relative to periodic orbits. Moreover, the possible trajectories of a massless particle are categorised based on its energy. Within the spatial CR3BP, for a given JC, JC_0, a five-dimensional energy surface is found within a six-dimensional phase space. The regions where a massless body with JC_0 can move in a system characterised by a gravitational constant μ are determined by projecting this energy surface into the rotating frame's positional space. These regions are traditionally called Hill regions, with their boundaries referred to as Zero Velocity Curves
(ZVCs), which denote points where the massless particle's kinetic energy is zero.

3. Candidates for the analysis

In a three-body system, it is possible to identify several families of periodic orbits [6, 7, 8], and this specifically applies to the CR3BP, as mentioned above. Of all the orbital families that can be defined within the CR3BP framework, this article will focus on Near Rectilinear Halo Orbits (NRHOs), specific branches of Halo families, both in L_1 and L_2. They are of particular interest for missions that aim to observe the lunar surface or analyse the characteristics of the Moon in general, as well as for human-crewed missions. What makes these orbits remarkable is not only their proximity to the Moon, but also their comparatively higher degree of linear stability with respect to other members of the same family [9]. In fact, the majority of NRHOs exhibit a Stability Index (SI) slightly above unity, which classifies them as linearly unstable periodic orbits [10], yet they remain close to the stability threshold, typically within the range $1 \leq SI \leq 8$. In this work, a subset of these orbits has been selected as a starting point for analysis and comparison of the two different disposal methods considered. Two NRHOs in EM-L_2 and two in EM-L_1 are selected as starting points for the analysis. The characteristics of such orbits are reported in the Table 1:

The same four orbits are also reported in Figure 1, as a function of the phase angle.

Orbit type	$JC\,[-]$	$SI\,[-]$	$r_p\,[km]$
NRHO in EM-L_2	3.0268	1.6908	8026.2
	3.0461	1.3652	3324.8
NRHO in EM-L_1	3.0025	2.0318	9756.5
	2.9926	6.0073	2563.5

Table 1. Characteristics of NRHOs candidates for the analysis: JC, SI and r_p, perilune radius.

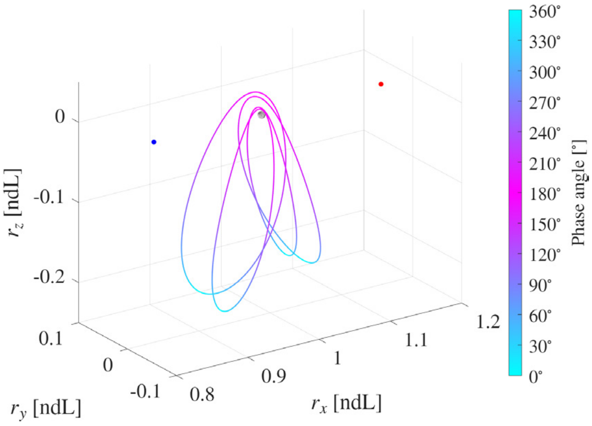

Fig. 1. NRHOs candidates for the analysis.

In the Figure, L_1 is denoted by the blue dot, while L_2 is indicated by the red dot. The phase angle is defined as:

$$\theta = \frac{2\pi t}{T} \tag{6}$$

The four candidate orbits are selected to provide representative examples spanning different values of the Jacobi constant, perilune radius, and stability index, thereby offering a preliminary indication of how the disposal results by varying with these parameters. The second NRHO around L_2 considered in this study, $JC = 3.0461$, closely resembles the orbit chosen as operational for the lunar Gateway. Additional insights into the interdependence of these key parameters can be found in [9].

4. Disposal theoretical framework

This section provides a concise overview of the theoretical framework adopted to design the two disposal strategies under consideration. The first focuses on heliocentric disposal, while the second addresses disposal through controlled lunar impact.

4.1 Heliocentric disposal

Heliocentric disposal consists of designing two-impulse low-cost trajectories departing from a periodic orbit in the EM system and transiting through EM-L_2. Trajectories should then reach SE-L_1 or, preferably, SE-L_2, and escape the ZVCs of the SE system. Finally, to ensure that the spacecraft cannot return in the EM vicinity, the ZVCs of the SE system must be closed, making re-entry theoretically impossible within the framework of the SE CR3BP. The European Space Agency (ESA) guidelines for the protection of the cislunar environment further require verification, through long-term simulations in an ephemeris-based dynamical model (including all major perturbations of the system), that the spacecraft remains outside the EM neighbourhood for at least 100 years. This last point is not addressed in this context and will be subject of a future work. The main challenge in designing heliocentric disposal for an EM periodic orbit in the CR3BP framework lies in how and when to account for the Sun's influence. This can either be included in the analysis from the beginning by exploiting, for example, the Bicircular Restricted Four-Body Problem (BR4BP), as done in [5], or by coupling the two three-body systems as in [11]. The approach adopted here will be the latter.

Initially, an unstable periodic orbit (in this case, a NRHO) is defined within the EM system. A first impulse is applied to the spacecraft along the direction of the unstable manifold of the periodic orbit, computed as a function of the eigenvector associated with the largest eigenvalue of its monodromy matrix [12]. The magnitude of this initial impulse is fixed a priori in the present analysis to reduce the number of varying parameters. After this initial impulse, the unstable manifold is propagated, and among its two branches, the one yielding the largest fraction of trajectories reaching EM-L_2 is selected. Trajectories leading to lunar impact, Earth impact, or failing to escape through EM-L_2 within ten months are discarded from further analysis. Manifold trajectories are propagated up until passing through EM-L_2. Once outside the ZVCs of the EM system, the spacecraft trajectories are still propagated in the EM CR3BP until the influence of the Moon becomes negligible compared to that of the Sun. The exact point at which the connection between the two dynamical models should take place is not uniquely defined in literature, and more dedicated analyses would be required to establish a precise criterion. In this work, the formulation proposed by Castelli [13] is adopted: in the coupled CR3BP, the transition from the EM to the SE CR3BP occurs when, if modelled within the BR4BP framework, the effect of the Moon becomes negligible compared to that of the Sun on the trajectory. Conversely, for transitions from the SE CR3BP back to the EM CR3BP, it must be determined when the Sun's influence becomes negligible compared to that of the Moon. The two dynamical models are connected through a coordinate transformation: all three bodies are approximated as coplanar, with the Moon's orbit assumed to lie in the ecliptic; and both the Earth's motion around the Sun and the Moon's motion around the Earth are approximated as circular. These approximations strongly affect the results, but they also simplify the formulation by requiring only one angle, rather than two, to define the relation between the two rotating reference frames, as expressed in Figure 2, where the subscript in indicates a generic inertial frame.

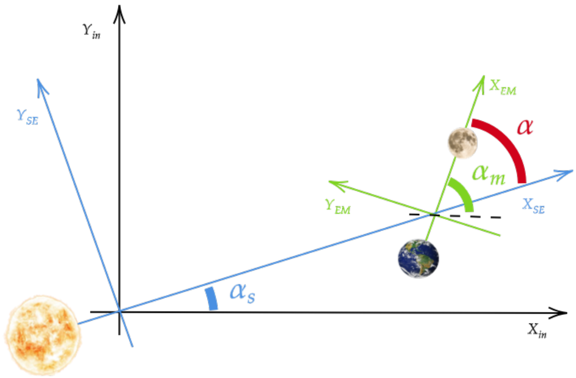

Fig. 2. Approximation considered to model the relationship between the SE and the EM rotating frame.

The angle α, defined as the difference between α_m, related to the EM system, and α_s, related to the SE one, is used to compute the geometric relationships between the two rotating systems, knowing that:

$$\alpha = \alpha_0 + \frac{\omega_{EM} - \omega_{SE}}{\omega_{EM}} t_{EM} \tag{7}$$

defines the evolution of the angle α in the EM system, being ω_{EM} and ω_{SE} the non-dimensional angular velocities of the two rotating frames, respectively; t_{EM} the non-dimensional time in the EM system at which α has to be computed; and α_0 the initial value of α, evaluated at the starting time t_0. The value of α_0 is so computed considering the relative position of the three celestial bodies at a certain fixed departure date, selected as April 15^{th} 2029. The dependence of the results on the departure time will be further investigated in future work. Using complex notation, to convert a position in the EM system to one in the SE:

$$\begin{cases} \boldsymbol{b_{SE}} = \dfrac{l_{EM}}{l_{SE}}\, e^{i\alpha}\, \boldsymbol{b_{EM}} + 1 - \mu_{SE} \\ r_{z_{SE}} = \dfrac{l_{EM}}{l_{SE}}\, r_{z_{EM}} \end{cases} \tag{8}$$

where

$$b_{SE} = r_{x_{SE}} + i\, r_{y_{SE}} \qquad b_{EM} = r_{x_{EM}} + i\, r_{y_{EM}} \tag{9}$$

and l_{EM} and l_{SE} are respectively the characteristic lengths of the EM and SE systems. To transform a velocity vector from the EM to the SE system:

$$\begin{cases} \dot{\boldsymbol{b}}_{\boldsymbol{SE}} = \dfrac{l_{EM}}{l_{SE}} \dfrac{\omega_{EM}}{\omega_{SE}} e^{i\alpha} \Bigg(i \left(1 - \dfrac{\omega_{SE}}{\omega_{EM}}\right) \cdot \\ \qquad \boldsymbol{b_{EM}} + \dot{\boldsymbol{b}}_{\boldsymbol{EM}} \Bigg) \\ v_{z_{SE}} = \dfrac{l_{EM}}{l_{SE}} \dfrac{\omega_{EM}}{\omega_{SE}}\, v_{z_{EM}} \end{cases} \tag{10}$$

To perform the inverse transformation (from SE to EM), it is sufficient to invert the equations.
The coupled CR3BP dynamical model is therefore defined as a framework that accounts for both the EM and SE-CR3BP formulations, switching from one to the other depending on the region of space in which the spacecraft is located: if the effect of the Moon on the trajectory dominates over the one of the Sun, the EM-CR3BP is used; conversely, if the solar effect is stronger, the SE-CR3BP applies. The coupling is so achieved through the coordinate transformations described above, together with a dynamical model switch based on the prevailing gravitational effects on the spacecraft's trajectory.
Once in the SE framework, the spacecraft trajectory is propagated and, if it reaches and exits through SE-L_2 or SE-L_1, a second impulse is applied to close the SE system ZVCs, thus preventing the spacecraft from reentering them. The magnitude of this impulse is defined through an energy-based approach: it is computed as a function of the spacecraft velocity at the point of the ZVCs closure and the difference between the trajectory's JC, as evaluated in the SE system, and that of SE-L_2 [4, 12].

4.2 Controlled lunar impact

Disposal through controlled lunar impact is achieved by designing trajectories that depart from a periodic orbit in the EM system and lead to a collision with the lunar surface. In this framework, only the EM-CR3BP is considered. This represents an approximation, since close to the Moon the influence of its gravitational harmonics becomes non-negligible. Nevertheless, the results obtained here provide a reasonable first-order estimate of the time and ΔV budget required for controlled lunar impact disposal. The inclusion of lunar gravitational harmonics in the dynamical model will be the subject of future work.

The disposal trajectories are modelled as three-impulse transfers, optimised to minimise the total ΔV while ensuring impact with the Moon. The optimisation is carried out through a multiple-shooting Sequential Quadratic Programming (SQP) algorithm, where the lunar impact condition is explicitly enforced as a constraint. The first manoeuvre is applied in the direction of the unstable manifold associated with the selected periodic orbit, thereby exploiting the natural system dynamics. In this case, the manifold branch passing closest to the Moon immediately after departure is selected. The magnitude of the initial ΔV is, as in the previous case, predetermined. Once injected onto the unstable manifold, the spacecraft naturally tends to approach the Moon closely. The role of the multiple-shooting algorithm is to apply small corrections to the manifold trajectories to guarantee lunar impact.
In principle, a single impulse along the unstable mani-

fold, coupled with a second impulse to correct the trajectory and impact the Moon would already be sufficient to drive the spacecraft onto a lunar-impact trajectory. However, the multiple-shooting approach generally facilitates convergence and enables targeting of lower-ΔV solutions. Nonetheless, the algorithm also allows for the possibility of a two-impulse disposal strategy, comprising the initial unstable manifold injection and a subsequent correction burn, if such a solution emerges as optimal.

Apart from the lunar impact constraint, additional conditions are imposed to avoid impacting protected regions. The Moon represents not only a scientific target of primary importance, but also a cultural and historical heritage that, similar to natural ecosystems on Earth, must be preserved. Current guidelines in this respect are not always universally agreed upon; however, for the present study, two main constraints have been considered:

- **Avoidance of impacts in the proximity of historical sites.** The recommendations provided in [14] strongly suggest preventing impacts within a radius of at least 2 km around these areas, such as the Apollo landing sites. It is also recommended to overfly these sites only with a trajectory tangent to the lunar surface, i.e., not overfly them during the descent phase, which can be translated into avoiding impact sites with similar longitudes and higher latitudes. This precaution reduces the probability that material released by the spacecraft during the disposal phase, or the plume generated by its propulsion, may contaminate or damage the historical landing areas. In this work, historical landing sites from the Apollo, Luna, Surveyor, Chang'e, Grail and LADEE missions are considered in the analysis. Data about such landing sites are retrieved from the Reconnaissance Orbiter Camera (LROC) database [15][14].

- **Avoidance of areas of particular interest for science and future missions.** The Committee on Space Research (COSPAR) establishes that special planetary protection guidelines should be applied in the case of landings or impacts within Permanently Shadowed Regions (PSRs) or near the lunar poles, specifically at latitudes further South of 79°S and further North of 86°N [16]. Consequently, it appears unreasonable to design a disposal strategy that would result in an impact within these regions. A latitude constraint is therefore introduced, which effectively excludes impacts at the poles. As for PSRs, since the majority of them are located near the poles, they are already implicitly excluded by this latitude constraint. For this reason, no additional constraints are currently imposed. However, future work will need to establish a comprehensive catalogue of PSRs and explicitly include them among the no-impact zones, in the same way as has been done for historical lunar sites.

As previously specified, the analysis is conducted considering the spacecraft subject only to the EM CR3BP dynamics, i.e., within the EM rotating frame. Upon lunar impact, constraints on longitude and latitude are imposed to ensure the avoidance of protected regions. The impact states are expressed in the Mean-Earth/Principal-Axis (ME/PA) reference frame, the standard convention used in lunar cartography. The departure date from the reference periodic orbit is considered fixed and is always equal to April 15^{th} 2029. Please note that the same date was used as a reference for the spacecraft's departure from the periodic orbit in the heliocentric disposal case. The impact time is then defined as this date plus the Time of Flight (ToF) for disposal. Further analysis will be conducted in future work to investigate the eventual dependence of the results on the departure date, particularly the final impact locations.

5. Simulations and results

In this section, the results obtained from the implementation of the two disposal strategies are presented. Particular attention is given to behaviours considered of interest, while the main advantages and limitations of each method are discussed.

5.1 Heliocentric disposal

In this section, the results obtained for the heliocentric no-return disposal strategy are presented. As a first case, the disposal of a spacecraft departing from the NRHO in L_2 with $JC = 3.0268$ is analysed. Among all the orbits considered in this study, this one is the closest to EM-L_2, and therefore represents the scenario in which heliocentric disposal is theoretically the most straightforward to implement.

The unstable manifold associated with the orbit is computed, and the branch directing the majority of trajectories toward EM-L_2 is selected. The perturbation required to insert the spacecraft onto the unstable manifold is typically set to be very small, with $\varepsilon \approx 10^{-4} - 10^{-6}$ in the EM system, corresponding to an initial ΔV_1 on the order of about $10^{-2} - 10^{-4}$ m/s. This perturbation should be small enough not to violate linearity but large enough to represent a perturbation to the periodic motion. However, the magnitude of ε influences both the outcome of the disposal and the ToF related to a certain solution. In this case, since escape from the SE system is required, not only from the EM one, a relatively large ΔV_1 is necessary to have a reasonable number of escapes. For this reason, the initial perturbation ε is selected equal to 10^{-4}, corresponding to an initial ΔV_1 of about $5 \cdot 10^{-2}$ m/s in the direction of the unstable manifold. The magnitude of ΔV_1 is fixed for

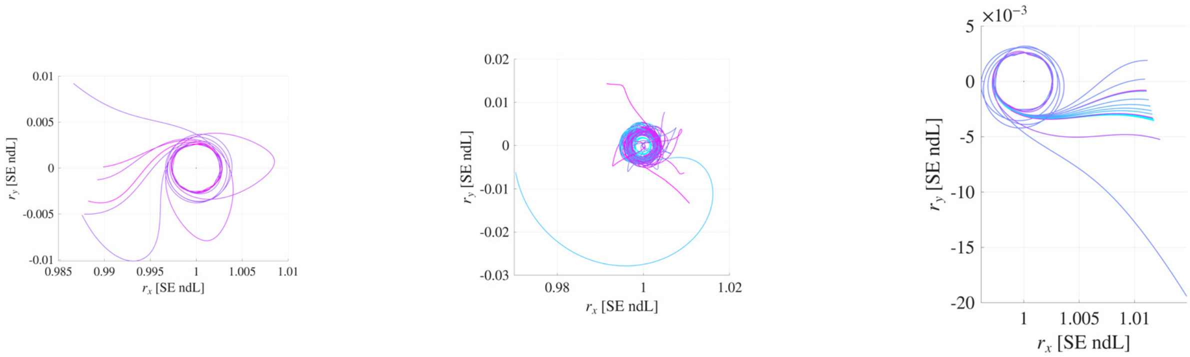

Fig. 3. Behaviour of disposal trajectories, NRHO in EM-L_2, $JC = 3.0268$, SE rotating frame, from left to right: escape through SE-L_1, no-escape in the ToF considered, escape through SE-L_2.

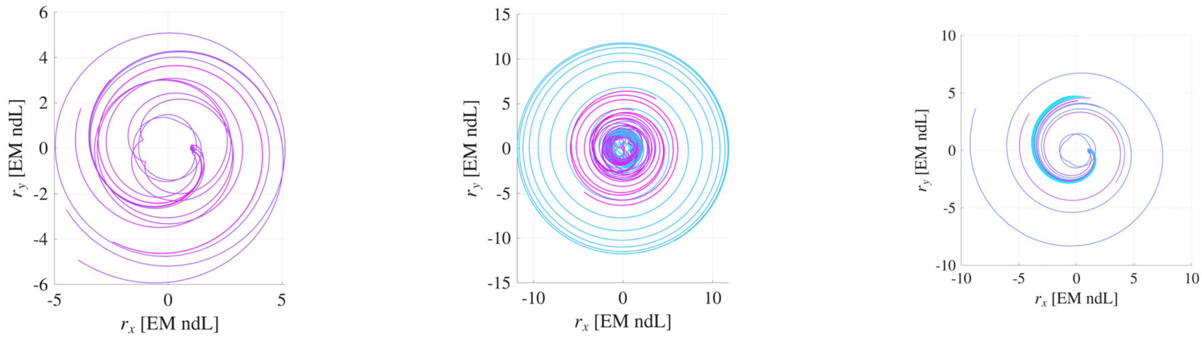

Fig. 4. Behaviour of disposal trajectories, NRHO in EM-L_2, $JC = 3.0268$, EM rotating frame, from left to right: escape through SE-L_1, no-escape in the ToF considered, escape through SE-L_2.

the overall analysis. As specified in previous Sections, the departure date is also fixed, which implies that the initial phase angle α_0, defining the relative positions of the Sun, the Earth and the Moon, is the same for all the cases considered in this analysis. This represents a relevant parameter that was observed to influence the results strongly, and which will therefore be the subject of further investigation and optimisation in future work. Trajectories leading to either Earth or Moon impact, or remaining confined within cislunar space for more than ten months, are discarded from further consideration. For all subsequent analyses, the maximum disposal ToF is fixed to ten months. Although this upper bound is large compared to the typical dynamical timescales of the cislunar environment and to standard operational needs, it was adopted to explicitly evaluate how the disposal ToF affects the overall results.

Once outside the ZVCs of the EM system, trajectories are propagated forward in time in either the EM or the SE CR3BP, depending on the object's instantaneous position. Propagation continues until one of the following conditions is met:

- escape through SE-L_1;
- escape through SE-L_2;
- the total ToF reaches ten months without the spacecraft leaving the Earth's neighbourhood.

These three possible behaviours are illustrated in the SE rotating reference frame in Figure 3 and in the EM rotating frame Figure 4 for the case under analysis. Lengths expressed in the SE rotating frame are reported in units of SE non-dimensional length (SE ndL), while those in the EM rotating frame are expressed as a function of the EM non-dimensional length (EM ndL). All trajectories are shown as a function of the phase angle of their departure point along the reference NRHO, using the same colour map defined in Figure 1.

From Figure 3, where the disposal trajectories are displayed in the SE rotating frame, the three different behaviours can be clearly distinguished. A first observation, which will also be highlighted later, is that no evident, clear correlation emerges between the phase angle at departure and the final behaviour shown. Among the possible outcomes, the most desirable one corresponds to the trajectories on the right-hand side of Figure 3: escape through SE-L_2. This guarantees that the spacecraft definitively leaves the SE system and, if the SE ZVCs are to be closed, this should prevent any possible reentry into the EM neighbourhood, as far as the CR3BP dynamical framework is considered. In this case, a fraction of the trajectories succeed in escaping the SE system in a reasonable time with a manoeuvre of roughly 0.05 m/s, excluding the additional ΔV required for ZVC closure.

Of the other outcomes, escape through SE-L_1 can still be considered as a potential disposal option, though it

presents some limitations not encountered in the SE-L_2 case. For example, a spacecraft disposed through SE-L_1 might still pose a residual risk to missions directed toward the Sun. However, since the primary objective of this work is to satisfy safety constraints in cislunar space, escape via SE-L_1 is treated as a viable, but secondary, option while escape through SE-L_2 is identified as the preferred and more reliable disposal strategy.
Finally, the behaviour shown by the graph at the centre of Figure 3 represents trajectories that never escape the Earth's neighbourhood. Of the three, this is the least advisable option, as it simply means disposal is unsuccessful. It is also interesting to observe how the trajectories shown in the SE rotating frame appear when represented in the EM rotating frame, by comparing Figure 3 with Figure 4. When the distance between the trajectory and the centre of mass of the system increases exponentially, the satellite can escape through SE-L_1 or L_2 of the SE system. In contrast, trajectories that, for the overall ToF considered, remain constrained around the EM centre of mass are the same for which disposal is unsuccessful.
Focusing now on the case in which trajectories propagated from the reference NRHO succeed in escaping the vicinity of the EM system through SE–L_1 or SE–L_2, once the ZVCs have been crossed, it is possible to modify the spacecraft's energy with a second manoeuvrer, ΔV_2, performed in the anti-tangential direction with respect to the local velocity, to change the JC of the trajectory, effectively closing the ZVCs and preventing the spacecraft from re-entering the vicinity of the EM system. This manoeuvre can only be performed after the ZVCs have been crossed and their external region has been reached. This implies the existence of a minimum time limit before which the manoeuvre cannot take place; however, once outside the ZVCs, the spacecraft can continue flying for a certain ToF before executing the closure manoeuvre.
To compute the ΔV required to close the ZVCs as a function of an increasing ToF, the trajectories are propagated for a maximum total duration of ten months, even after one of the two Lagrangian points has been crossed. All escape trajectories, propagated over the full time interval considered, are reported in Figure 5: the velocity curves of the SE system computed at L_2 are shown in red, while the black dots indicate the instant of ZVC crossing, namely the first moment at which the closure manoeuvre becomes feasible.

In Figure 6, the total disposal ΔV evolution is reported as a function of the total disposal phase duration and the phase angle of the initial departure point from the reference NRHO.

The areas highlighted in orange correspond to trajectories that, within the ten-month propagation period considered, never succeed in passing through the SE–L_1 or SE–L_2 bottleneck regions. The areas marked in red correspond instead to trajectories that impact the Moon. Cases where a green bar is present before the beginning of the colour map related to the ΔV evolution

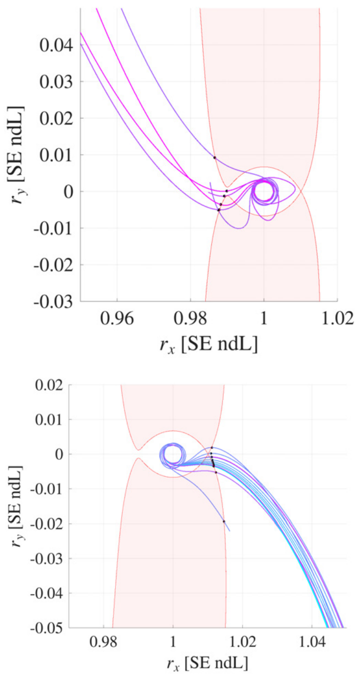

Fig. 5. Behaviour of disposal trajectories, NRHO in EM-L_2, $JC = 3.0268$, SE rotating frame. Upper graph: trajectories escaping through SE–L_1. Lower graph: trajectories escaping through SE–L_2.

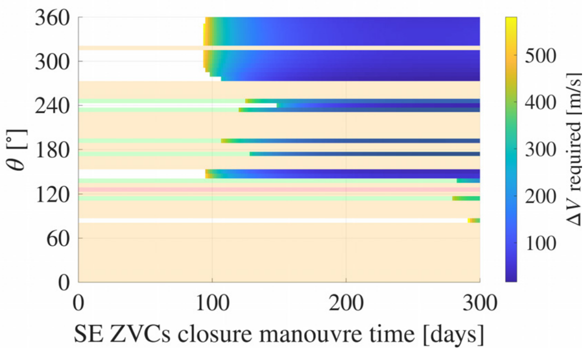

Fig. 6. Evolution of the total disposal ΔV as a function of the total disposal phase duration and the phase angle of the initial departure point from the reference NRHO in EM-L_2, $JC = 3.0268$.

indicate escapes through L_1 rather than L_2. All remaining cases correspond to escapes through L_2.
On the left-hand side of the plot, the graph is empty even for the successful cases: for low ToF values, disposal is not feasible, as neither SE–L_2 nor SE–L_1 has yet been crossed. Once the crossing occurs, the disposal cost is initially very high, and then decreases progressively as the ToF increases. This behaviour is consistent with what was observed in [12] for escape trajectories from EM–L_2 that do not return to the vicinity of the EM system. In addition, the costs required to close the ZVCs appear overall to be quite large: even after allowing for significant ToFs, the total cost of the dis-

posal phase remains on the order of 50 m/s. This result is reasonable, as the analysis focuses on a NRHO located very close to the Moon, which is already disadvantaged with respect to other orbits when attempting to escape the EM system. The energy gap to be covered is therefore substantial, resulting in a considerable ΔV_2 required to close the ZVCs when only the SE CR3BP is considered. This ΔV value is obtained by considering only the SE CR3BP. It can be hypothesised that, by adopting more complete gravitational models that account for the effect of multiple bodies in the system, it may be possible to identify more favourable energetic conditions, enabling the closure of the velocity curves with significantly lower ΔV requirements. This aspect will also be the subject of future work. Finally, the percentage of trajectories for which disposal is successful is of the 39.34%.

The evolution of disposal trajectories for the NRHO in EM-L_2 with $JC = 3.0461$ is not reported here, since it is essentially similar to what was observed in the previous case. The overall evolution of disposal trajectories, together with that of the total ΔV as a function of the ToF and the phase angle, is reported in Figure 7.

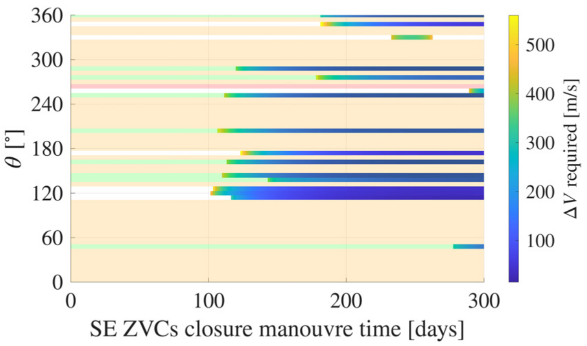

Fig. 7. Evolution of the total disposal ΔV as a function of the total disposal phase duration and the phase angle of the initial departure point from the reference NRHO in EM-L_2, $JC = 3.0461$.

The overall behaviour is broadly similar to what was observed in the previous case. The main difference is that, in this case, far fewer trajectories can escape. Since the orbit considered here lies even closer to the Moon compared to the previous one, many manifold trajectories fail to escape the EM system altogether. Moreover, the minimum disposal ToF is even higher than in the previous case, especially for some local solutions. This indicates that some trajectories orbit for a long time in the Earth's neighbourhood before escaping, which is not an advisable behaviour. Overall, the percentage of success is lower in this case, within the conditions chosen for the analysis. The percentage of cases in which disposal is successful is the 26.23%.

In Figure 8 and Figure 9, the disposal trajectories obtained from the analysis considering the NRHO around L_1 with $JC = 3.0025$ are shown, represented in the SE and EM rotating frames, respectively. The corresponding results for the NRHO around L_1 with $JC = 2.9926$ are not reported here, as they are overall similar to those obtained for the first L_1 NRHO case. The final results for the analysis are reported for the NRHO in L_1 with $JC = 3.0025$ in Figure 10, for the one with $JC = 2.9926$ in Figure 11.

The behaviour of the disposal trajectories is overall consistent with what was observed in the previous cases. The key difference, when considering a NRHO around L_1, lies in the significant number of trajectories that either impact the Moon or fail to escape the EM ZVCs. Both phenomena occur with non-negligible frequency. This can be attributed to the highly non-linear dynamics in the vicinity of these orbits and to the fact that, when escaping from EM–L_2, manifolds departing from L_1 NRHOs must pass through a region where the gravitational influence of the Moon is strong. As a result, it is reasonable to expect that, without any other adjustment, an impact with the Moon may eventually occur. For the NRHO with $JC = 3.0025$, the percentage of successful disposals is 36.07%, for the one with $JC = 2.9926$ is 9.8%.

5.2 Controlled lunar impact

The controlled lunar impact disposal option for the L_2 NRHO with $JC = 3.0268$ is considered. Successful disposal trajectories, computed through the optimisation algorithm, are reported in Figure 12.

In Figure 12, the disposal trajectories are reported using the same colour map as in Figure 1, again plotted as a function of the phase angle of the departure point. In this case, the disposal trajectories have been optimised to minimise ΔV, while incorporating constraints to ensure lunar impact and to avoid protected areas. A maximum ToF of 20 days has been imposed, which has been considered reasonable as it limits the number of revolutions the trajectory could perform around the Moon before impact. From an operational standpoint, longer ToF scenarios are not realistic, given the strong perturbations caused by the Moon's gravitational field in this region.

The first manoeuvre point corresponds to the insertion onto the unstable manifold, and therefore lies directly on the orbit. Since its position is fixed, the points at which the first of the manoeuvres for each of the trajectories is applied are not reported in the graph. The second and third manoeuvre points are indicated, respectively, with red and green dots in the Figure. It is noteworthy that many of the points where the third manoeuvre is applied occur at the apolune of the trajectories. This is reasonable from a trajectory design perspective, as the objective of the design is to lower the perilune of the manifold, which naturally approaches the Moon in the case of NRHOs, until an impact is obtained. The second manoeuvre, on the other hand, occurs over a broader region of the orbit in terms of θ. Interestingly, in most cases, it

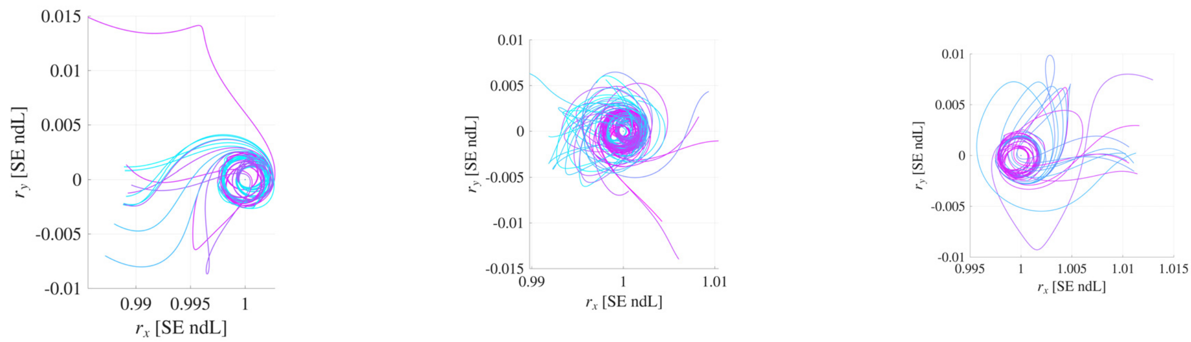

Fig. 8. Behaviour of disposal trajectories, NRHO in EM-L_1, $JC = 3.0025$, SE rotating frame, from left to right: escape through SE-L_1, no-escape in the ToF considered, escape through SE-L_2.

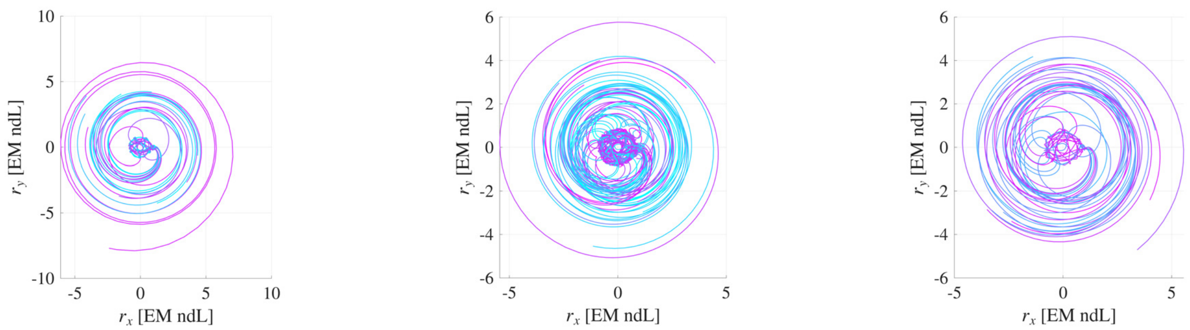

Fig. 9. Behaviour of disposal trajectories, NRHO in EM-L_1, $JC = 3.0025$, EM rotating frame, from left to right: escape through SE-L_1, no-escape in the ToF considered, escape through SE-L_2.

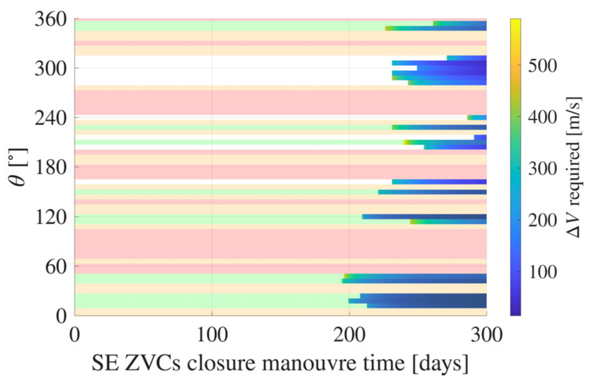

Fig. 10. Evolution of the total disposal ΔV as a function of the total disposal phase duration and the phase angle of the initial departure point from the reference NRHO in EM-L_1, $JC = 3.0025$.

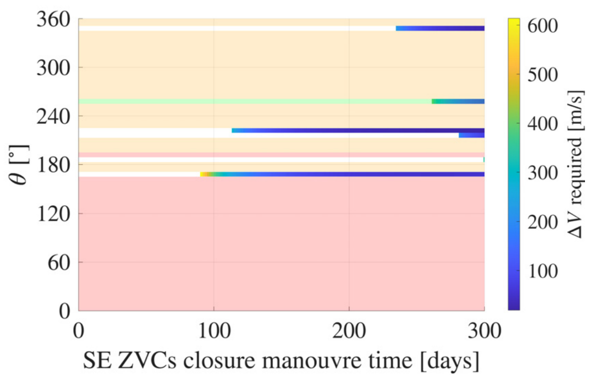

Fig. 11. Evolution of the total disposal ΔV as a function of the total disposal phase duration and the phase angle of the initial departure point from the reference NRHO in EM-L_1, $JC = 2.9926$.

takes place almost immediately after the insertion into the unstable manifold. To clarify the corresponding impact locations, the latitude and longitude of the impact points are reported in Figure 13, together with the protected regions.

In this case as well, the impact points are reported on the map as a function of the phase angle of the departure point. The red areas at the top and bottom of the graph indicate latitude regions where satellite impacts are not allowed, with their limits fixed by the black dashed line, while the red circles denote the locations of historical sites. It is important to note that the circle of 2 km radius around the historical sites, within which impacts must be avoided, is represented by the small black dot at the centre of the red circles in the graph. The red circles are shown for illustrative purposes only; theoretically, the no-impact zones are much smaller. All impact points are largely confined to the same area in this case, with their distribution evolving according to the phase angle, as clearly observable from the graph. Figure 14 reports

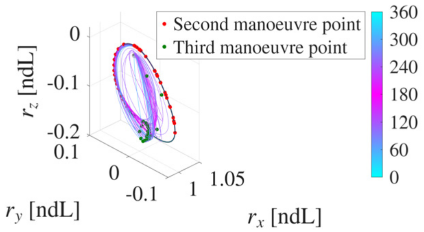

Fig. 12. Controlled lunar impact disposal trajectories, L_2 NRHO with $JC = 3.0268$.

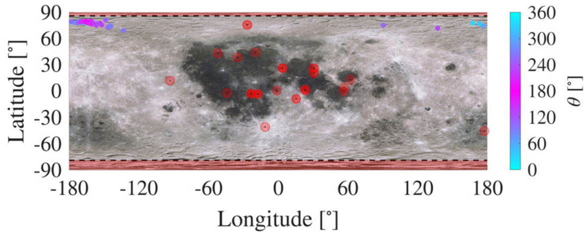

Fig. 13. Impacts locations on the Moon, L_2 NRHO with $JC = 3.0268$.

the evolution of ΔV as a function of both ToF and phase angle for the different cases considered.

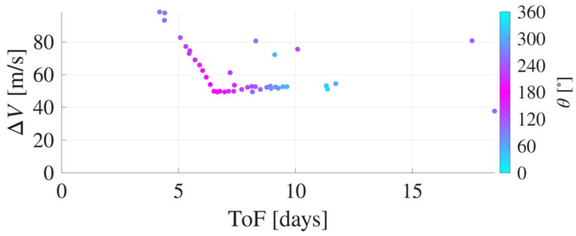

Fig. 14. Disposal with impact on the Moon ΔV evolution as function of the TOF and phase angle, L_2 NRHO with $JC = 3.0268$.

The mean ΔV required for a controlled lunar impact is approximately 50 m/s, with a mean ToF of approximately 7 days. The evolution of ΔV and ToF as a function of the phase angle is clearly visible in the graph, with the region of lower ΔV and ToF corresponding to trajectories departing from phase angles around 180°. It is reasonable to expect that this ΔV could be further reduced if the perturbations due to the Moon's gravitational field are taken into account. This point will be addressed in future work. It is also important to note that these results are based on the specific input parameters selected for this simulation. Further analysis will be conducted to understand how to properly tune the magnitude of the first manoeuvre, ΔV_1, and the date of orbit departure, as well as to optimise the algorithm constraints and parameters to achieve more even favourable outcomes. Finally, it is important to note that only successful disposal trajectories are reported in the graphs. Of the trajectories considered in this case, 67.21% were successful.

The evolution of disposal trajectories, impact sites, and ΔV versus ToF are reported, respectively, in Figure 15, Figure 16, and Figure 17 for the L_2 NRHO with $JC = 3.0461$.

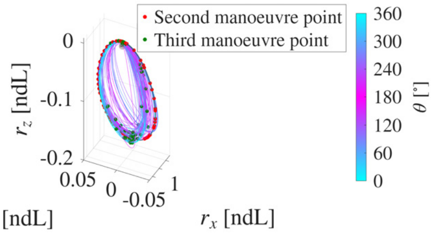

Fig. 15. Controlled lunar impact disposal trajectories, L_2 NRHO with $JC = 3.0461$.

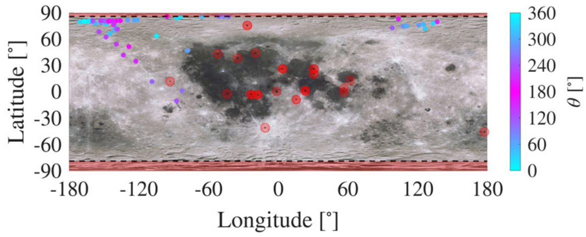

Fig. 16. Impacts locations on the Moon, L_2 NRHO with $JC = 3.0461$.

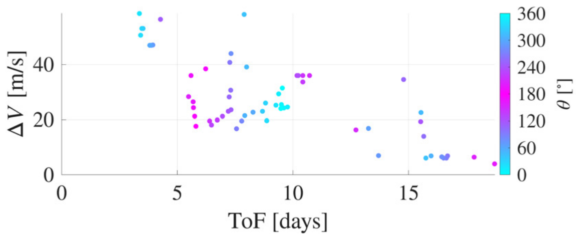

Fig. 17. Disposal with impact on the Moon ΔV evolution as function of the TOF and phase angle, L_2 NRHO with $JC = 3.0461$.

First, it is noteworthy that, as in the previous case, the majority of the third manoeuvres occur at the apolunes of the trajectories. The mean ΔV required for the disposal trajectories is lower than in the previous case, approximately 15 m/s, while the mean ToF remains similar at around 6–7 days. In this case as well, the most promising solutions correspond to departures from a point on the NRHO at a phase angle of 180°, i.e., at perilune. Compared to the previous case, the solutions are considerably more scattered both in terms of ΔV and ToF, as well as with respect to the impact locations. Nevertheless, all successful impacts occur within safe regions. The increased dispersion of the results reflects an enhanced capability of the algorithm to find different solutions and optimise them relative to the previous case: with more ways to adjust the trajectory while respecting the constraints, the algorithm can identify a greater variety of feasible solutions, thereby minimising the disposal ΔV more effectively than before. This can be justified, first of all, by the lower perilune of the nominal orbit, which is much lower with respect to the previous case. Also, the percentage of successful trajectories was 100%.

Proceeding to the analysis of the results obtained for NRHOs around L_1, the trajectory evolution, impact sites, and ΔV versus ToF are reported in Figure 18, Figure 19, and Figure 20 for the NRHO in L_1 with $JC = 3.0025$.

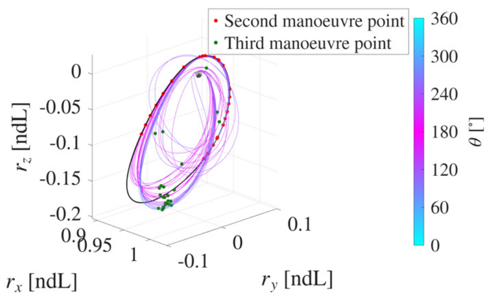

Fig. 18. Controlled lunar impact disposal trajectories, L_1 NRHO with $JC = 3.0025$.

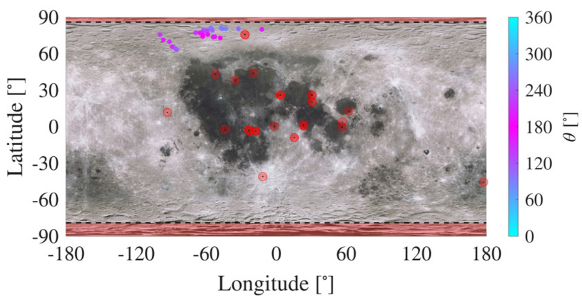

Fig. 19. Impacts locations on the Moon, L_1 NRHO with $JC = 3.0025$.

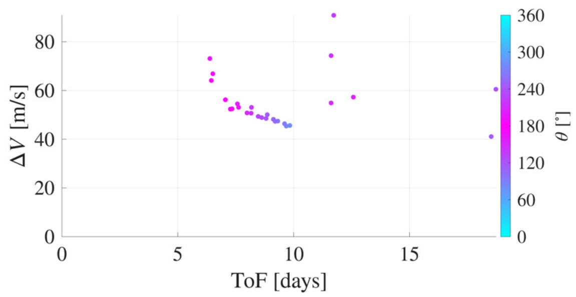

Fig. 20. Disposal with impact on the Moon ΔV evolution as function of the TOF and phase angle, L_1 NRHO with $JC = 3.0025$.

In this case, the evolution of the disposal trajectories is highly chaotic, as shown in Figure 18. Nevertheless, the majority of the third manoeuvre points are located at the apolunes of the disposal trajectories. The impact site map indicates that the situation is similar to that observed for the first of the NRHO around L_2 considered: the mean cost for the disposal phase is approximately 50 m/s, with a mean ToF of about 8–9 days. To depart at the NRHO perilune seems the most promising option, too. Furthermore, most of the solutions are clustered in the same region in both the impact sites map and the ΔV versus ToF graph. This suggests a certain rigidity in the algorithm, which is capable of identifying solutions only in the vicinity of a specific trajectory evolution, apart from a few local exceptions. This is also the case in which this type of disposal is the least successful, with only 44.26% of the disposal trajectories achieving success.

In Figure 21, Figure 22 and Figure 23, the results related to the L_1 NRHO with $JC = 2.9926$ are reported.

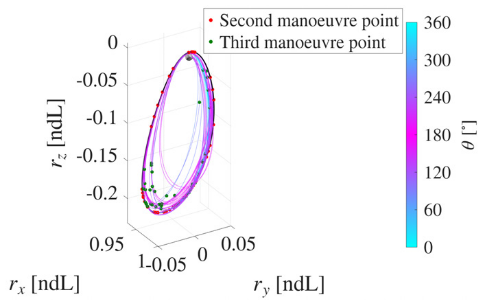

Fig. 21. Controlled lunar impact disposal trajectories, L_1 NRHO with $JC = 2.9926$.

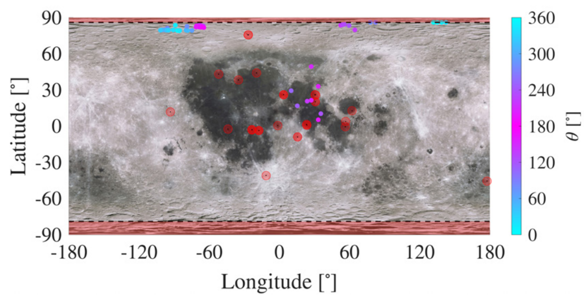

Fig. 22. Impacts locations on the Moon, L_1 NRHO with $JC = 2.9926$.

In this case, where the NRHO perilune is lower compared to the previous one, the ΔV and ToF generally required for disposal are reduced. As observed for the second NRHO considered around L_2, the results in both the impact sites and the ΔV versus ToF graphs are highly scattered, indicating that the solution space is diverse and that the algorithm can identify a wide variety of feasible solutions. Consequently, some impact sites exhibit significantly different longitudes and latitudes compared to others. Nevertheless, all reported solutions satisfy the imposed constraints.

The mean ΔV required for disposal is approximately 17 m/s, with a mean ToF of about 7 days. Two distinct fam-

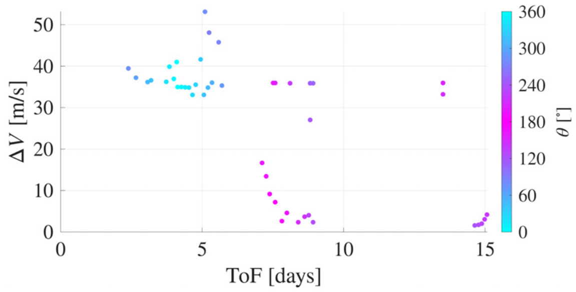

Fig. 23. Disposal with impact on the Moon ΔV evolution as function of the TOF and phase angle, L_1 NRHO with $JC = 2.9926$.

ilies of solutions can be identified. The first corresponds to phase angles around $0°$, departing from the apolune of the NRHO, which requires a higher ΔV but a shorter ToF, reaching very high latitudes. The second family features lower ΔV and longer ToF, reaching lower latitudes, with departure from the NRHO perilune. In this latter case, it is important to carefully consider the constraint of avoiding historical sites, ensuring that all solutions comply with this requirement. Finally, in this case, the 73.77% of cases analysed is successful.

6. Conclusions and future works

In this work, two EoL disposal strategies for spacecraft operating in EM NRHOs around L_1 and L_2 have been analysed and compared. These orbits are of particular interest for both scientific and operational missions. However, their greater stability compared to other Halo orbits, together with their proximity to the Moon, makes the design of disposal strategies more complex.
Two disposal methods are investigated: heliocentric disposal through escape no-return trajectories; and controlled lunar impact, ensuring that protected regions and historical sites are avoided. Both approaches yielded preliminary but promising results, although the influence of several relevant parameters has not been fully accounted for in the present analysis. For heliocentric disposal, further investigation is needed on the relationship between the relative phase of the three bodies in the system and escape trajectories, such as that between the initial ΔV_1 magnitude and the final disposal result. Similarly, for lunar impact disposal, extending the analysis to multi-impulse trajectories and refining the initial guesses for the optimisation algorithm could further reduce both the total ΔV and the ToF, while increasing the overall disposal success rate.
Overall, the results obtained suggest that controlled lunar impact generally requires a lower ΔV budget and shorter ToFs compared to heliocentric disposal. Nonetheless, the heliocentric option could be safer than the lunar impact one, and still offers a wider space for improvement, as the influence of many parameters on the results remains to be systematically analysed. For the design of both disposal options, the dynamical model should also be further refined. In the case of heliocentric disposal, this involves assessing the potential influence of additional celestial bodies on the system, whereas for lunar impact disposal, it requires incorporating the effects of the Moon's gravitational harmonics into the analysis.

7. Acknowledgements

This research has received funding as part of the work developed for the agreement n. 2023-37-HH.0 for the project "Attività tecnico-scientifiche di supporto a C-SSA/ISOC e simulazione di architetture di sensori per SST", established between ASI, Italian Space Agency, and POLIMI, Politecnico di Milano.

References

[1] "Gateway - NASA," https://www.nasa.gov/mission/gateway/. Last accessed: 21 August 2025.

[2] "Artemis mission - NASA," https://www.nasa.gov/humans-in-space/artemis/. Last accessed: 21 August 2025.

[3] "ESA Space Debris Mitigation Requirements," Tech. rep., ESA Space Debris Mitigation Working Group, 2023, Available: ESA Space Debris Mitigation Requirements.

[4] Olikara, Z. P., Gómez, G., and Masdemont, J. J., "Dynamic mechanisms for spacecraft disposal from Sun-Earth libration points," *Journal of Guidance, Control, and Dynamics*, Vol. 38, No. 10, 2015, pp. 1976–1989, doi: 10.2514/1.G000581.

[5] Boudad, K. K., Davis, D. C., and Howell, K. C., "Disposal trajectories from Near Rectilinear Halo Orbits," *AAS/AIAA Astrodynamics Specialists Conference, Portland, Maine*, 2018.

[6] Szebehely, V., *Theory of Orbit: The restricted problem of three Bodies*, Academic Press, 1st ed., 1967.

[7] Doedel, E. J., Romanov, V. A., Paffenroth, R. C., Keller, H. B., Dichmann, D. J., Galán-Vioque, J., and Vanderbauwhede, A., "Elemental periodic orbits associated with the libration points in the circular restricted 3-body problem," *International Journal of Bifurcation and Chaos*, Vol. 17, No. 08, 2007, pp. 2625–2677, doi: 10.1142/S0218127407018671.

[8] Hénon, M., *Generating Families in the Restricted Three-Body Problem, II. Quantitative Study of Bifurcations*, Springer Berlin, Heidelberg, 2003, doi: https://doi.org/10.1007/3-540-44712-1.

[9] Bolis, M., Alessi, E. M., and Colombo, C., "Long-Term Evolution of Orbits in Cislunar Space: Characterisation and Stability Analysis," *International Astronautical Conference (IAC), Milan, Italy*, 2024.

[10] Connor Howell, K., "Three-dimensional, periodic,'halo'orbits," *Celestial mechanics*, Vol. 32, No. 1, 1984, pp. 53–71, doi: https://doi.org/10.1007/BF01358403.

[11] Van der Weg, W. J. and Vasile, M., "Sun-Earth L_1 and L_2 to Moon transfers exploiting natural dynamics," *Celestial Mechanics and Dynamical Astronomy*, Vol. 120, No. 3, 2014, pp. 287–308.

[12] Bolis, M., Alessi, E. M., and Colombo, C., "End-of-life disposal parametric analysis in cislunar space: Earth-Moon L2 escape no-return trajectories," *9th European Conference on Space Debris, Bonn, Germany*, 2025.

[13] Castelli, R., *On the Relation Between the Bicircular Model and the Coupled Circular Restricted Three-Body Problem Approximation*, chap. 1, Springer New York, 2011.

[14] "NASA's Recommendations to Space-Faring Entities: How to Protect and Preserve the Historic and Scientific Value of U.S. Government Lunar Artifacts," 2011, Authored by Human exploration and operations mission directorate strategic analysis and integration division NASA headquarters.

[15] "Lunar Reconnaissance Orbiter Camera," Avaible at: https://lroc.im-ldi.com/featured_sites. Last accessed: 10-9-2025.

[16] "COSPAR policy on planetary protection," 2021, Authored by COSPAR Panel on Planetary Protection and approved by the COSPAR Bureau.